JACS
JOURNAL OF THE AMERICAN CHEMICAL SOCIETY
pubs.acs.org/JACS
Article

De Novo Design of High-Performance Cortisol Luminescent Biosensors

Julie Yi-Hsuan Chen,[‖] Xue Peng,[‖] Chenggang Xi, Gyu Rie Lee, David Baker, and Andy Hsien-Wei Yeh*

Cite This: *J. Am. Chem. Soc.* 2025, 147, 27494−27505
Read Online

ACCESS | Metrics & More | Article Recommendations | Supporting Information

ABSTRACT: Frequent, reliable cortisol measurement is critical for diagnosing and managing adrenal disorders, stress responses, and circadian rhythm disruptions. However, current cortisol assays or detection methods remain confined to laboratory settings, limiting on-site testing. Protein-based biosensors provide a promising point-of-care (POC) solution, yet no robust, field-ready protein-based cortisol biosensor is available. Here, we de novo design cortisol-inducible dimerization modules and systematically sample their fusions with split luciferase reporters by using a protein structure prediction pipeline. The resulting biosensor, designed straight from the computer, yields over 300-fold luminescent response with picomolar sensitivity and can be rapidly imaged by a standard camera or smartphone. This work highlights the power of computational protein design for developing next-generation protein-based biosensors.

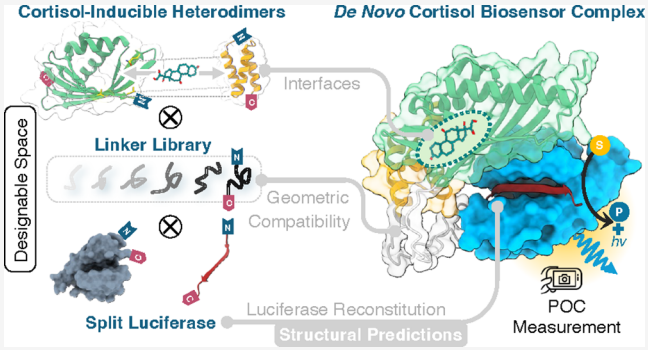

Downloaded via UNIV OF WASHINGTON on October 8, 2025 at 17:39:04 (UTC).
See https://pubs.acs.org/sharingguidelines for options on how to legitimately share published articles.

■ INTRODUCTION

Cortisol, a steroid hormone produced by the adrenal glands, plays a critical role in various physiological processes such as stress response, immune modulation, blood pressure, and sleep-wake cycle regulations that are essential for maintaining health.[1] Monitoring cortisol levels is important for diagnostics because cortisol imbalances can indicate adrenal disorders, e.g., excess cortisol leads to Cushing's Syndrome,[2] and insufficient cortisol causes Addison's Disease.[3] In addition, abnormal cortisol rhythms can disrupt the sleep-wake cycle, and elevated cortisol is linked to the degree of stress levels and metabolic disorders.[4] Monitoring cortisol levels frequently can also guarantee patients' outcomes when undergoing treatment for adrenal disorders to ensure proper dosing and effectiveness.[5] However, standard methods for cortisol detection are restricted to enzyme-linked immunosorbent assay (ELISA) or liquid chromatography-tandem mass spectrometry (LC-MS) that have to be performed in laboratory settings, while point-of-care methods for frequent, on-site testing in clinics or at-home remain limited or are at the proof-of-concept stage.[6]

Protein-based biosensors have emerged as a promising modality for detecting clinically relevant analytes in solution using a mix-and-read format.[7] This approach eliminates the need for multiple washing and incubation steps by leveraging analyte-induced conformational changes in the sensing protein, which directly modulate the activity of the linked reporter protein module.[8,9] Incorporating luciferase enzyme as the optical reporter has demonstrated ultrasensitive detection in complex specimens such as blood and urine.[10] Unlike fluorescence, enzyme-catalyzed luminescence does not require external excitation, reducing the background noise from autofluorescence and scattering in biological matrices. This self-emitting light signal also simplifies detection, enabling the use of simple devices, such as a camera, to capture signals from paper-imprinted biosensors.[11,12] These advantages make luminescent protein biosensors highly suitable for cost-effective point-of-care diagnostics.

Designing a cortisol luminescent protein biosensor requires two components: a recognition domain that binds cortisol (Figure 1a) and undergoes significant conformational changes; and a reporter system, such as split luciferase, that generates a detectable signal upon reconstitution. However, naturally occurring cortisol-binding proteins, such as corticosteroid-binding globulin[13] and the glucocorticoid receptor,[14] either lack substantial conformational changes upon cortisol binding or possess complex folding patterns that hinder biosensor development. To overcome these limitations, we sought to design cortisol-responsive protein dimerization systems from scratch using computational de novo protein design. These designer proteins dimerize in the presence of cortisol, bringing split luciferase domains into proximity to form reconstituted

Received: March 24, 2025
Revised: July 10, 2025
Accepted: July 11, 2025
Published: July 28, 2025

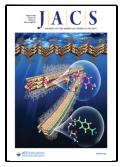

© 2025 The Authors. Published by American Chemical Society

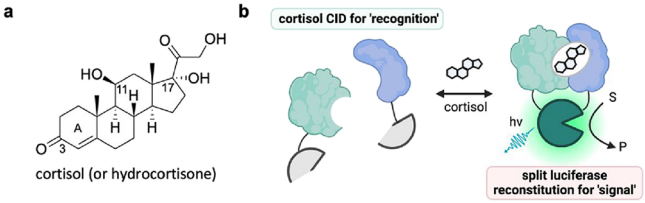

Figure 1. Cortisol-responsive, protein-based biosensor design. (a) Chemical structure of cortisol (hydrocortisone), showing the steroidal core and functional groups. (b) Illustration of the binary cortisol biosensor consisting of a cortisol-inducible heterodimerization module (blue and green), each fused to the complementary fragments of a split luciferase system (gray). In the presence of cortisol, the reconstituted luciferase emits detectable luminescence, enabling the direct measurement of cortisol levels in solution.

and active luciferases, which produce luminescence (Figure 1b).

The first component for building a luminescent cortisol biosensor is designing cortisol-induced dimerization systems. Chemically induced dimerization (CID) systems are valuable tools in synthetic biology for controlling specific cellular functions, such as transcription, protein degradation, and enzyme activation, with high spatiotemporal precision.[15] However, the availability of native CID systems remains limited. Among the identified systems, only the rapamycin-induced FKBP-FRB system has been widely adopted in mammalian systems due to the small size of FKBP and FRB proteins (12 and 11 kDa, respectively) and their nanomolar binding affinity for rapamycin, forming a highly stable ternary complex.[16] In contrast, plant-derived CID systems, such as abscisic acid-induced ABI-PYL[17] and gibberellin-induced GID-GAI,[18] are not always effective across multiple biological systems, likely due to suboptimal protein folding. Rational design of new CID systems remains challenging as it requires creating ternary complexes involving two proteins and a small molecule. Previous computational approaches for CID design rely on pre-existing protein heterodimer interfaces,[19] native ligand−protein complexes,[20−22] or by splitting de novo designed proteins that bind to small molecules.[23] Here, we present a stepwise computational strategy to design both dimerization proteins individually, yielding two well-folded de novo proteins that interact with a cortisol ligand to form newly designed ternary interfaces at nanomolar affinity. This design approach allows precise control over protein geometries, streamlining the creation of CID systems tailored for split luciferase fusion protein biosensor design.

Besides, we developed a protein structure prediction pipeline to sample geometrically compatible orientations between the dimerization domains and split luciferase components, facilitating efficient fusion protein design. This work demonstrates that de novo protein design can enable the creation of custom functions by explicitly designing corresponding protein structures, eliminating the need to rely on naturally occurring proteins. As a result, our structure-guided design strategy successfully developed high-performance luminescent protein-based biosensors capable of detecting cortisol at physiological and pharmaceutical concentrations with point-of-care compatible settings.

■ RESULTS

Computational Design and Characterization of Cortisol-Induced Protein Dimerization. We previously utilized a large number of de novo NTF2 scaffolds to design small-molecule protein binders against six structurally distinct small molecules.[24] Among these, we successfully obtained hcy129.1 binder that binds cortisol with nanomolar K_D, which falls within the physiological concentration range of cortisol in the body. The ligand-bound crystal structure closely matched that of both the designed and AlphaFold2-predicted models, suggesting our ability to design protein−ligand interfaces accurately. In the designed structure, hcy129.1 engaged the core steroid structure of cortisol, leaving the 3-carbonyl group and adjacent carbon atoms of steroid ring A exposed to the solvent (Figure 2). We reasoned that designing another 'lid'

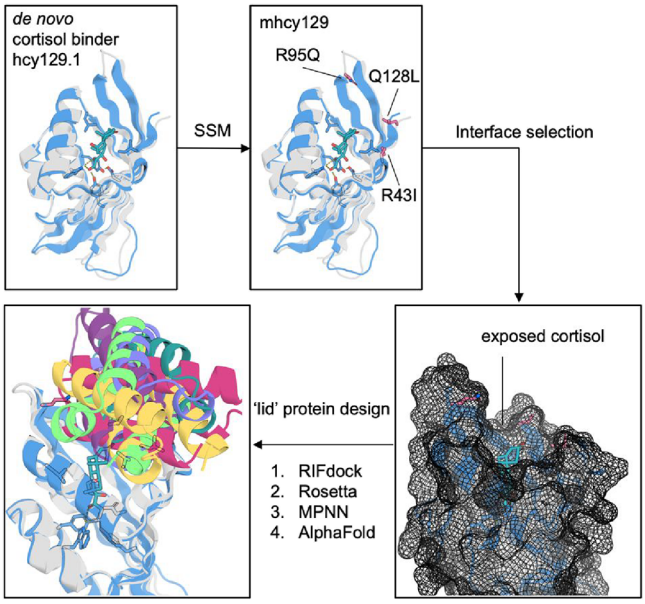

Figure 2. Workflow for the design of cortisol-inducible dimerization. The de novo cortisol binder hcy129.1 (top left) was first engineered via site-saturation mutagenesis (SSM) at three positions (R43I, R95Q, Q128L) to yield mhcy129 (top center), retaining nanomolar cortisol affinity but exposing the A-ring handle of cortisol for targeted 'lid' protein binding (bottom right). Using RIFdock, Rosetta, ProteinMPNN, and AlphaFold2 prediction, multiple lid scaffolds were docked and designed against this exposed cortisol interface (bottom left), forming new ternary complexes that assemble in the presence of cortisol. More computational design details are provided in Figure S2. The white model represents the designed hcy129.1-cortisol complex, while the blue model shows the AlphaFold prediction of mhcy129, indicating that the overall structure remains intact following the introduction of triple mutations.

protein to specifically cover the interface of the hcy129.1-cortisol complex, without binding hcy129.1 alone, could create a cortisol-dependent CID system. To facilitate binder design, we first introduced three mutations (R43I/R95Q/Q128L) into hcy129.1 based on the site saturation mutagenesis (SSM) map (Figure S1a). Such modifications remove charged and polar residues that could obstruct the binding interface design toward the hcy129.1-cortisol complex. The resulting triple mutant, named mhcy129, retained a similar folding profile and nanomolar binding affinities to cortisol compared to the parent hcy129.1 (Figure S1b,c).

To design cortisol-dependent CID systems, we used RIFdock to place 'lid' protein scaffolds against the open mhcy129-cortisol complex interface (Figure 2). A library of previously described helical bundles[25] was docked explicitly to

https://doi.org/10.1021/jacs.5c05004
J. Am. Chem. Soc. 2025, 147, 27494−27505

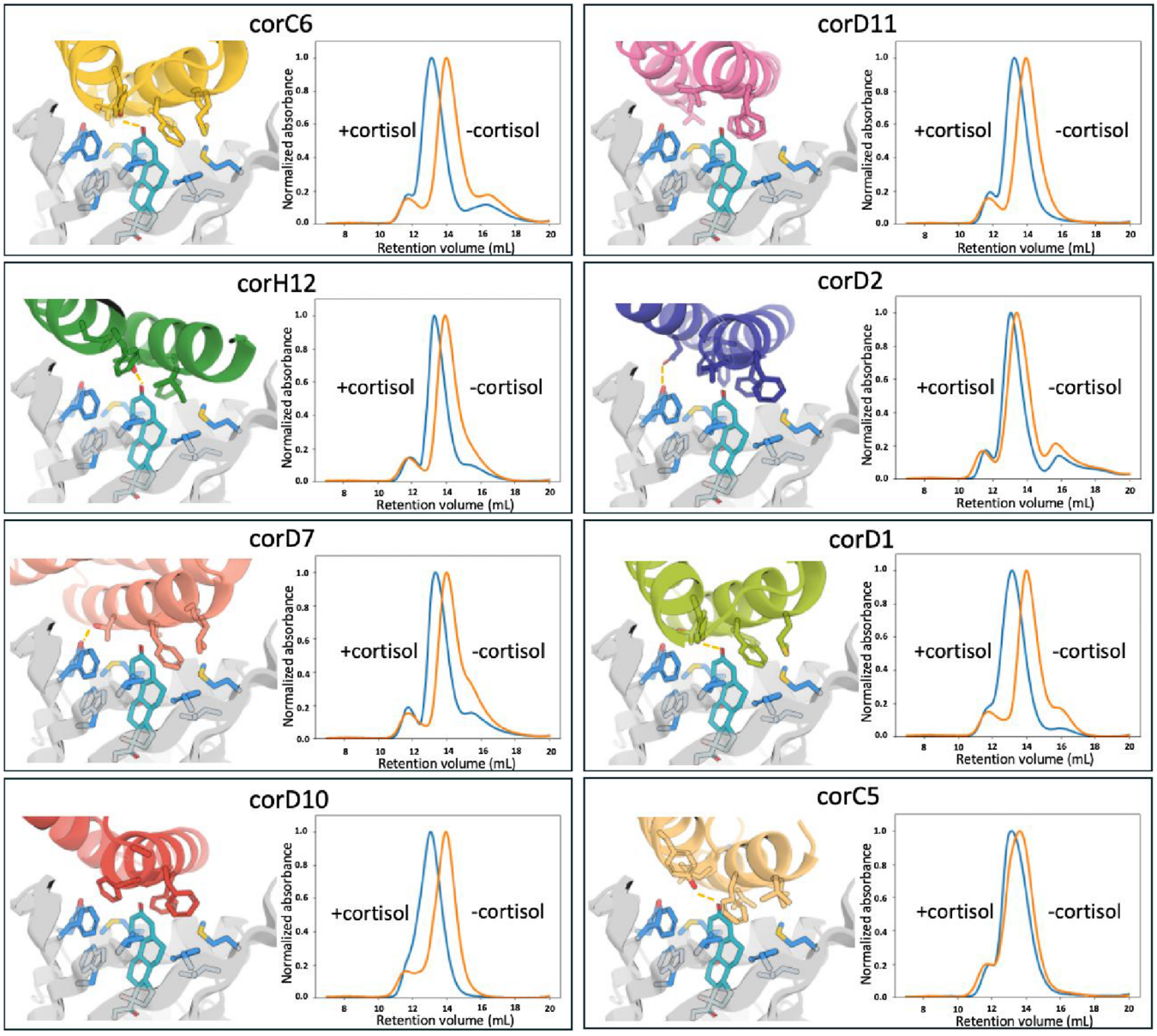

Figure 3. Designed models and size-exclusion chromatography (SEC) analysis of cortisol-inducible heterodimerizations. Each panel (left) illustrates a zoomed-in view of the designed lid protein (colored ribbons) to mhcy129 (gray) interface in complex with cortisol (teal). Key contacts were shown in sticks. A leftward shift in the elution volume of the corresponding SEC traces (right panel) in the presence (blue) compared to the absence (orange) of 10 μM cortisol indicated the formation of the ternary complex for each designed lid protein.

form contacts with the exposed cortisol interface. This docking strategy aimed to generate numerous ternary complexes by making contacts with the cortisol ligand, where mhcy129 and the lid proteins interact only in the presence of cortisol to minimize ligand-independent dimerization. Subsequently, we performed sequence design on the docked complexes using a combination of Rosetta FastDesign and ProteinMPNN.[26] The designed ternary complex structures were prefiltered by contact molecular surface (>440), Rosetta ddG (<−35), and contact patch with cortisol (>45). These filters aimed to ensure that the lid proteins formed enough physical interactions with both cortisol and mhcy129 (Figure S2). The designed heterodimeric complexes were further validated with AlphaFold2,[27] in which we selected models with pAE < 10 to assess interchain positioning confidence and pLDDT > 90 for the lid proteins. Although AlphaFold2's metrics (pAE and pLDDT) are reliable predictors for binder design,[28] its complex prediction is not explicitly aware of cortisol (all-atom protein models, such as RoseTTAFold-All-Atom[29] or AlphaFold3,[30] were not available at the time of designing). Thus, we complemented our computational design approach with experimental screening to further reduce the level of ligand-independent dimerization.

For experimental screening, we displayed the library containing designed lid proteins on the yeast surface and performed binding to biotinylated mhcy129, in which the FITC signal represented protein expression on the yeast surface, and the SAPE signal indicated binding of lid proteins to biotinylated mhcy129 (Figure S3a). In the first round of fluorescence-activated cell sorting (FACS), we collected populations that expressed but did not bind to mhcy129. In the following rounds, we treated the yeast cells with cortisol

https://doi.org/10.1021/jacs.5c05004
J. Am. Chem. Soc. 2025, 147, 27494−27505

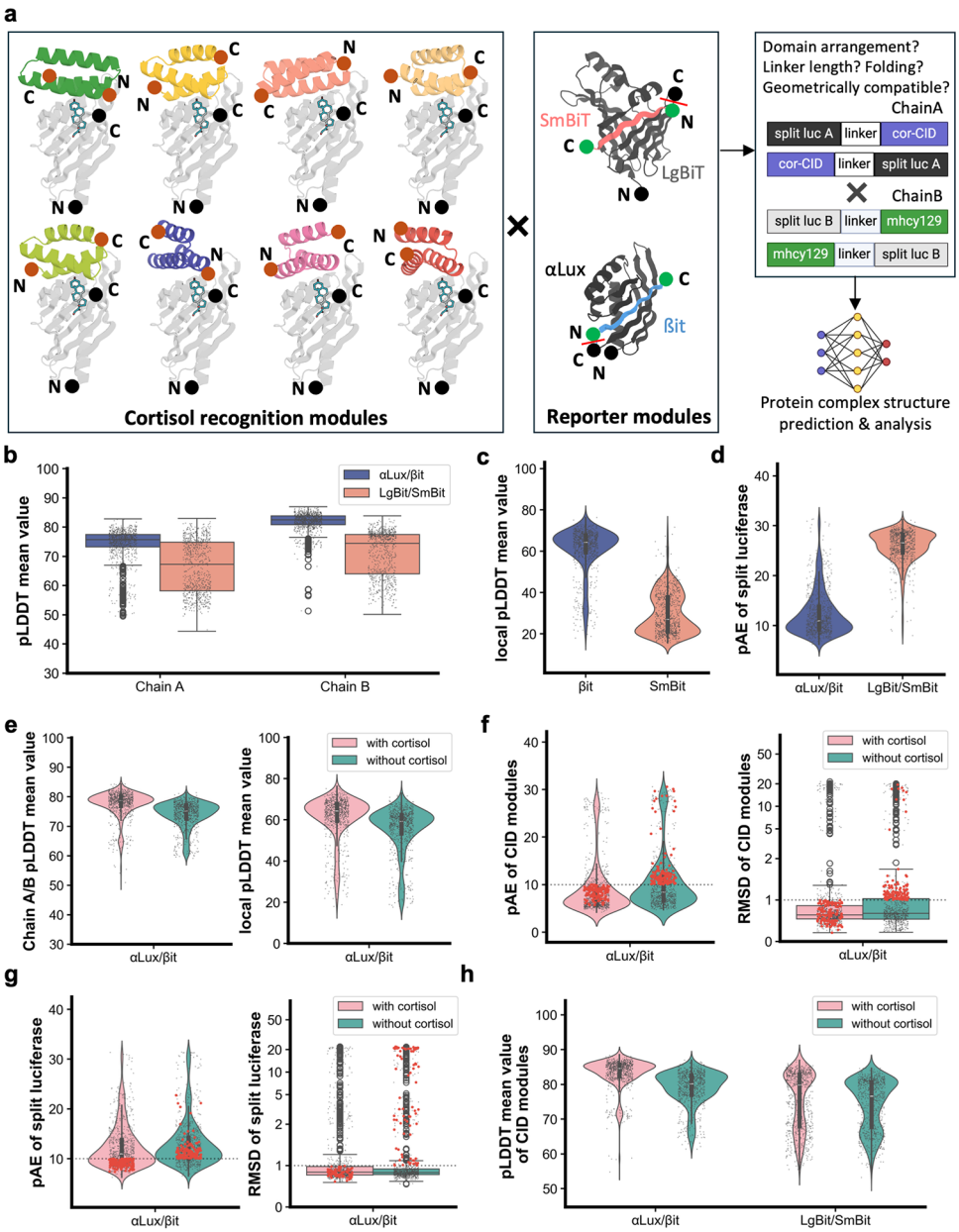

Figure 4. Computational sampling of the fusion protein space for cortisol CID modules with split luciferase reporters using structure prediction. (a) Schematic of the eight de novo designed cortisol CID modules (top left), each exhibiting distinct N/C orientations and topological variations. When paired with two different split luciferase reporters (LgBiT/SmBiT and αLux/βit; top center), the resulting fusion proteins span a broad combinatorial design space. Large-scale protein complex predictions were used to assess domain arrangement, linker length, and overall folding. (b−d) Comparison of AlphaFold3-derived metrics for the predicted protein biosensor complexes by evaluating the (b) mean pLDDT scores of chains A and B, (c) local pLDDT specifically in βit or SmBiT regions, and (d) local predicted Alignment Error (pAE) for the reconstituted αLux/βit or LgBiT/SmBiT luciferases. (e−g) Analysis of predicted complexes with or without cortisol by comparing (e) the mean pLDDT of the entire chain A-B complexes (left) and the βit region alone (right); pAE and calculated Cα rmsd for (f) the CID modules or for (g) the split luciferase reporter (αLux/βit) domains. Red points marked predicted models where pAE scores >10 or Cα rmsd >1 Å in the absence of cortisol but fall below these thresholds in the presence of cortisol. (h) Comparison of the mean pLDDT for the CID modules when fused to αLux/βit (left) or LgBiT/SmBiT (right) split luciferases, both with and without cortisol. A breakdown analysis of individual CID is provided in Figure S5.

during binding to biotinylated mhcy129 and collected the enriched populations that exhibited mhcy129 binding in a cortisol-dependent manner (Figure S3b). Next, we randomly picked 96 single yeast colonies from the collected populations and validated each with FACS for mhcy129 binding in the presence and absence of cortisol (Figures S3c and S4). Through this process, we identified 35 lid proteins that showed cortisol-dependent binding signals by FACS. To confirm cortisol-dependent dimerization, we selected 10 lid proteins based on the largest difference in FACS signals between the presence and absence of cortisol (Figure S4), expressed and purified them from bacteria; 9 out of the 10 exhibited predominantly monodispersed and monomeric profiles in size exclusion chromatography (SEC) traces (Figure S4). We incubated each of the monomeric lid proteins with purified mhcy129 in the presence and absence of cortisol and analyzed the mixtures using SEC. Eight out of 10 lid proteins showed a cortisol-dependent shift in molecular size, suggesting that these

https://doi.org/10.1021/jacs.5c05004
J. Am. Chem. Soc. 2025, 147, 27494−27505

lid proteins form cortisol-inducible heterodimers with mhcy129 (Figure 3). By investigation of the structure of these designed lid proteins, all of them form highly complementary interfaces toward the mhcy129-cortisol complex and hold multiple contacts to the exposed A ring of cortisol. Thus, we successfully designed and verified cortisol-induced heterodimerizations using a hybrid computational and experimental strategy.

Constructing Cortisol Luminescent Biosensors by Structure Prediction. Traditionally, constructing functional protein biosensors required modifying native proteins through relooping, circular permutation, or trial-and-error linker engineering to explore different fusion configurations.[31] These approaches often disrupted protein folding and compromised function, so iterative rounds of directed evolution are generally required to restore functionality.[32] Furthermore, the inherent geometry of native proteins often imposes constraints, limiting the capacity to effectively test diverse configurations.

In contrast, de novo protein design allows the creation of lid proteins with diverse and tailored geometries, including variations in N- and C-terminal orientations, helical bundle topologies, and protein curvatures (Figure 4a, left panel). Such structural diversity expands the possible design space for genetic fusions of cortisol CID modules with split luciferases as the sensor reporter. To select the reporter module, we focused on two split luciferase systems: the NanoBiT system (LgBiT/SmBiT)[33] derived from engineered *Oplophorus* luciferase, and a new split luciferase system, LuxSit sPro (αLux/ßit) developed from a de novo designed luciferase.[34,35] Both systems are split at the last β-strand, producing two inactive fragments that reconstitute into a functional luciferase enzyme only when brought into close proximity by molecular dimerization (Figure 4a, middle panel).

To achieve a successful biosensor design, topologically compatible protein fusion between the cortisol CID and split reporter modules is critical. Proper alignment requires optimizing domain arrangement, linker length, and geometric compatibility to ensure effective reconstitution of the luciferase fragments upon cortisol-induced dimerization. Additionally, the final fusion proteins must maintain proper folding to preserve their functionality. With such diverse geometries of our designed cortisol CID systems, the combination of fusing cortisol recognition modules with split luciferase reporter modules presents a vast design space, which requires the sampling of a large number of possible configurations to satisfy important factors such as compatible domain arrangement, suitable linker length, and matched geometric orientation (Figure 4a, right panel).

To address this complexity, we sought to leverage AlphaFold3[30] structure prediction to systematically sample such a large designable space of these potential fusion proteins. This approach enabled us to evaluate geometric compatibility, folding stability, and 3D-spatial alignment between the cortisol recognition modules and split luciferase fragments in silico. For structure prediction, chain A comprised (i) split luciferase fragment A (αLux or LgBiT); (ii) a linker; and (iii) a designed lid protein, while chain B contained (i) split luciferase fragment B (ßit or SmBiT); (ii) a linker; and (iii) mhcy129. Both chains were designed to be similar in size (∼18−20 kDa). We evaluated two configurations for each chain (Figure 4a, right panel) with five linker lengths (1, 2, 4, 6, and 8 GS linkers; see Table S1), resulting in 2 (domain arrangement) × 5 (linker lengths) × 8 (cortisol CIDs) for chain A and 2 (domain arrangement) × 5 (linker lengths) × 1 (mhcy129) for chain B. We predicted the complexes of chain A and chain B in both the presence and absence of cortisol, yielding a total of 80 × 10 × 2 (plus/minus cortisol) = 1600 complex structures per split luciferase system.

After performing protein complex structure prediction, we evaluated the folding quality of the fusion proteins using AlphaFold3′s pLDDT score for each chain. The αLux/βit split luciferase system constantly exhibited a higher distribution of pLDDT values compared to the LgBiT/SmBiT system in both chains A and B (Figure 4b), suggesting higher prediction confidence for αLux/βit-based fusion proteins across eight designed cortisol CIDs (Figure S5a). For local prediction metrics, we analyzed the pLDDT and pAE scores at the βit or SmBiT regions. The βit region exhibited higher pLDDT values (Figures 4c and S5b), and the reconstituted αLux/βit complex showed lower pAE scores compared to those of the LgBiT/SmBiT system (Figures 4d and S5c). These results suggested that the αLux/βit split luciferase exhibits superior predicted structural confidence, relative to the LgBiT/SmBiT system, to form active luciferase upon cortisol binding.

As AlphaFold3 is an all-atom model that can handle nonprotein components, we compared the pLDDT of predicted chain A-B complexes with and without giving cortisol to AlphaFold3. Predictions including cortisol generally produced higher global and local pLDDT values, indicating that AlphaFold3 is sensitive to the presence of the ligand (Figures 4e and S5d,e). To validate the cortisol-dependent dimerization, we calculated the pAE values for mhcy129-CID complex regions and compared the CID Cα rmsd of the predicted complexes by aligning to our designed models (see Methods). Similar to what we observed, AlphaFold3 predicted the formation of mhcy129-CID complexes better when cortisol was present (Figures 4f and S5f). Notably, we successfully extracted models (red points) that had pAE > 10 (or Cα rmsd > 1 Å) in the absence of cortisol (meaning not forming mhcy129-CID complex), but pAE < 10 (or Cα rmsd < 1 Å) in its presence (meaning forming mhcy129-CID complex), which indicated that AlphaFold3 might be able to capture designed complexes preferentially in the presence of cortisol and reduce cortisol-independent dimerization at the in silico design stage.

To assess the luciferase reconstitution, we again calculated the pAE values and local βit Cα rmsd of the predicted reconstituted luciferase (αLux/βit) domains against reference structures (the designed LuxSit-i model[34]). Models based on the αLux/βit system consistently exhibited low pAE and Cα rmsd (Figures 4g and S5g), indicating more complete reconstitution of the luciferase domain and likely higher luciferase activity upon cortisol-induced dimerization. Similarly, we also observed predicted models (red points) with pAE > 10 (or Cα rmsd > 1 Å) in the absence of cortisol (incomplete luciferase reconstitution), but pAE < 10 (or Cα rmsd < 1 Å) in the presence of cortisol (fully reconstituted luciferase for signal), which together could be used to reduce cortisol-independent luciferase activity (background) and maximize the cortisol-dependent emission (signal) to design biosensors with large fold-of-changes (Figure S6).

Interestingly, AlphaFold3 consistently predicted the formation of mhcy129-CID ternary complex better when the presence of cortisol, regardless of which luciferase system was employed (Figures 4h and S5h), suggesting the robustness of our de novo designed cortisol CID modules. To summarize,

https://doi.org/10.1021/jacs.5c05004
J. Am. Chem. Soc. 2025, 147, 27494−27505

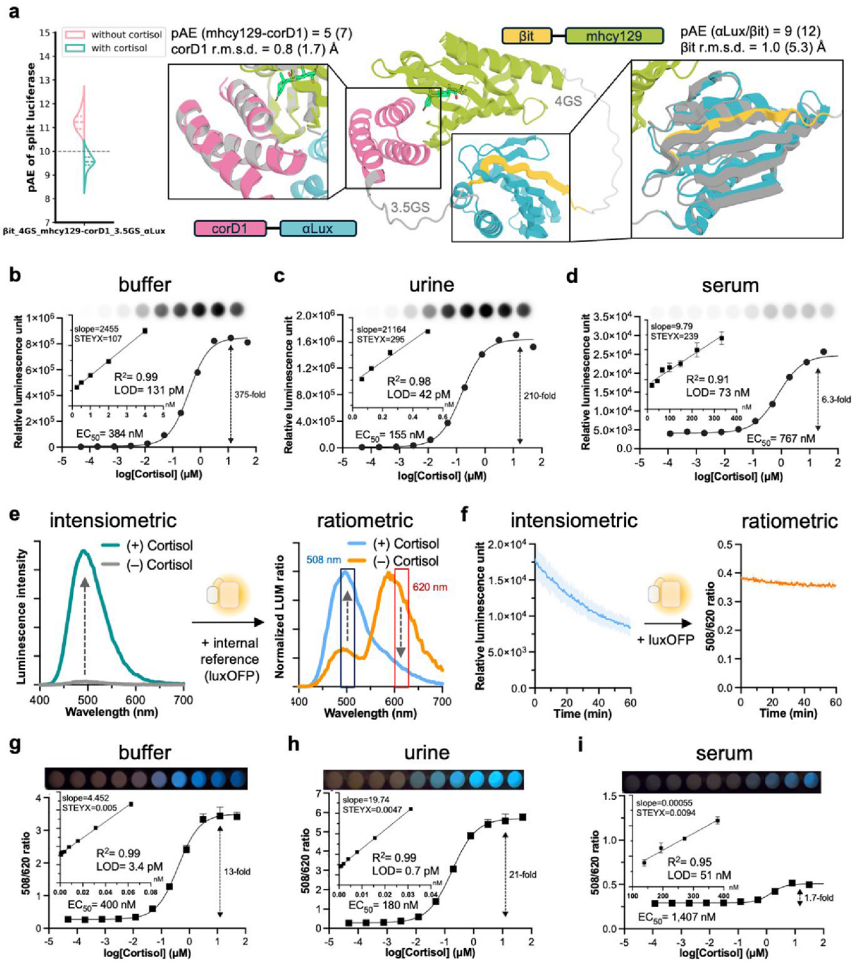

Figure 5. Computationally predicted structure, functional characterization, and applications of the designed cortisol biosensors. (a) Predicted binary complex biosensor model consists of corD1-3.5GS-αLux and βitsPro-4GS-mhcy129 proteins. Analysis of 160 predicted complex structures from AlphaFold3 reveals distinct pAE value distributions for the reconstituted αLux-βit domain in the presence and absence of cortisol (left panel). The low predicted pAE value of 5 for the mhcy129-corD1 complex indicates high confidence in cortisol-induced dimerization. Zoom-in views of the mhcy129-corD1 and αLux-βit interfaces show a close structural match with the designed CID module (rmsd = 0.8 Å) and the active LuxSit-i luciferase (rmsd = 1.0 Å, corresponding to the luminescence signal). The calculated rmsd values of αLux-βit complex with (1.0 Å) and without cortisol (5.3 Å) suggest that luciferase reconstitution is likely to occur in the presence of cortisol. (b) Cortisol response curves demonstrated that the corD1-3.5GS-αLux and βitsPro-4GS-mhcy129 pair (15 nM) achieved a 375-fold luminescence increase with a limit of detection (LOD) of 131 pM in HBS buffer; (c) 210-fold luminescence increase with a LOD of 42 pM in 20% synthetic urine; and (d) 6.3-fold luminescence increase with a LOD of 73 nM in 20% pooled human serum. Camera-captured images of the emitted signals are displayed at the top of each panel. (e) Conversion of the intensiometric signal to ratiometric detection is achieved by using an internal reference, luxOFP (Em max. = 588 nm). In the ratiometric mode, the signal ratio between the 508/20 and 620/40 nm channels increases as cortisol concentration rises. (f) Including the luxOFP internal reference enables correction of luminescence signal decay in 20% pooled human serum over time. The combination of corD1-3.5GS-αLux, βitsPro-4GS-mhcy129, and luxOFP enabled highly sensitive ratiometric cortisol detection. The biosensor exhibited 13-fold, 21-fold, and 1.7-fold ratiometric changes with detection limits of 3.4 pM, 0.7 pM, and 51 nM in (g) HBS buffer, (h) synthetic urine, and (i) human pooled serum, respectively. The top panel displays the color transition from orange to teal captured by a smartphone as the cortisol concentration increases, demonstrating wash-free and reliable on-site quantification. The standard error of the predicted Y-value in the linear regression (STEYX) was calculated in Excel, and LOD was calculated as 3 × standard error/slope.

the αLux/βit-based fusion proteins demonstrated higher prediction success rates than LgBiT/SmBiT in AlphaFold3. This likely stems from the well-folded nature of the αLux/βit system, developed from a de novo designed luciferase,[34] making it a promising reporter module for building luminescent cortisol biosensors.

To validate our prediction results, we experimentally constructed, expressed, and purified corD2-(1,2,4,6 GS linker)-αLux, αLux-(2,4,6 GS linker)-corD2, mhcy129-(1,2,4 GS linker)-βitsPro, and βitsPro-(1,2,4 GS linker)-mhcy129. Equal molar amounts of chains A and B were mixed in solution in the presence or absence of 10 μM cortisol, and the luminescence signal was measured using a plate reader. The experimental results closely matched the AlphaFold3 computational metrics, including pLDDT and pAE, which corresponded to the observed luminescence intensity and sensor fold-of-change (Figure S7). Additionally, AlphaFold3 successfully identified geometrically incompatible pairs, such as corD2-1GS-αLux/mhcy129-2GS-βitsPro and corD2-1GS-αLux/βitsPro-2GS-mhcy129, which exhibited poor reconstitution and minimal luminescence. These findings demonstrate the robustness of using an integrated structure prediction approach in systematically predicting optimal configurations, ensuring the formation of complex protein folding, maximizing

https://doi.org/10.1021/jacs.5c05004
J. Am. Chem. Soc. 2025, 147, 27494−27505

cortisol-induced reporter reconstitution, and streamlining the fusion protein design process for effective luminescent biosensors.

High-Performance Luminescent Cortisol Biosensors Designed Directly from Computer. Since the corD1 lid protein consistently showed superior predictions from computational analysis (Figure S5), we selected corD1 for more computational sampling across finer linker lengths (Figure S8). Based on the favorable pAE and rmsd values, we chose corD1-3.5GS-αLux/βitsPro-4GS-mhcy129 (Figure 5a) and corD1-3.5GS-αLux/mhcy129-4GS-βitsPro (Figure S9a) pairs for experimental evaluation. The in silico parameters collectively indicated high confidence in the cortisol-induced dimerization of the corD1-mhcy129 complex (pAE of corD1-mhcy129) and efficient luciferase reconstitution (pAE of αLux/βit and rmsd of βit or αLux/βit).

When we expressed corD1-3.5GS-αLux (Figure S9b), mhcy129-4GS-βitsPro (Figure S9c), βitsPro-4GS-mhcy129 (Figure S9d) along with the previous design based on the miniH11-NanoBit system,[24] we observed that the fusion proteins based on the αLux/βit binary system showed more monomeric and monodispersed protein folding profiles than LgBiT/SmBiT (Figure S9f,g). Additionally, SEC trace analysis showed a clear shift in retention time, suggesting that corD1-3.5GS-αLux and βitsPro-4GS-mhcy129 form a heterodimer triggered by the addition of cortisol (Figure S9e).

To assess the performance of our de novo biosensors for cortisol detection, we measured the luminescence signals of these biosensors with varying cortisol concentrations. The corD1-3.5GS-αLux/βitsPro-4GS-mhcy129 luminescent biosensor exhibited a 375-fold increase in emission with a limit of detection (LOD) of 131 pM (Figure 5b) while the corD1-3.5GS-αLux/mhcy129-4GS-βitsPro pair showed higher luminescence intensity at saturated cortisol concentrations along with a 153-fold change with a LOD of 82 pM (Figure S9h). Both biosensor pairs displayed a detection regime spanning over 4 orders of magnitude and significantly outperformed that of the previous NanoBiT-based design, which showed a 28-fold change with a LOD of 63 nM in HBS buffer (Figure S9i). Moreover, the designed corD1-3.5GS-αLux/βitsPro-4GS-mhcy129 biosensor maintained a robust 210-fold signal change with a LOD of 42 pM in synthetic urine (Figure 5c) and a 6.3-fold signal change with a LOD of 73 nM in human serum (Figure 5d). In contrast, the NanoBiT system showed a 21-fold change (LOD = 46 nM) in urine and a 2.8-fold change (LOD = 398 nM) in serum under identical conditions (Figure S9i). Although serum components attenuated the sensor performance, the broad dynamic range and high luminescence intensity of our designed biosensors still allowed for straightforward signal detection using a standard camera (Figure 5b−d).

To assess the target selectivity, we measured the dose-dependent responses of three structurally related steroid hormones (Figure S10a) using a corD1-3.5GS-αLux/βitsPro-4GS-mhcy129 luminescent biosensor. The sensor exhibited over 300-fold luminescence increase in response to cortisol, with lower responses to progesterone and aldosterone, and no detectable response to estradiol, illustrating moderate to strong target selectivity (Figure S10b). In addition, the sensor response is reversible as demonstrated by the time-course experiment, in which the presence of cortisol induced dimerization and luciferase reconstitution, while the removal of cortisol led to a reversal of the luminescence signal (Figure S10d). Similar to the other two-component biosensors,[7,36] our sensor exhibited a hook effect at high cortisol concentrations due to saturation of both dimerization protein interfaces (Figure S10e). The sensor response is also tunable by adjusting the concentration and ratio of the two protein components (Figure S10f).

To further improve quantitative measurement with better reliability and reproducibility, we introduced an internal reference, luxOFP,[37] into the assay to convert the intensiometric luminescence signal into ratiometric responses (Figure 5e). The maximum emission wavelength of luxOFP is 588 nm, which can be optically separated from the 490 nm emission of reconstituted αLux/βit luciferase using conventional filters. The ratiometric detection approach can correct for luminescence signal suppression in complex matrices[7−9] and normalize the luminescence decay to ensure the signal is stable over time (Figure 5f). By using luxOFP as the internal reference in the assay, we achieved ratiometric signal changes of 13-fold, 21-fold, and 1.7-fold in response to cortisol in buffer (Figure 5g), urine (Figure 5h), and serum (Figure 5i), with corresponding LODs of 3.4, 0.7, and 51 nM, respectively. This approach enabled more sensitive and reliable quantification of low cortisol concentrations (e.g., pico- to femtomolar range in urine) compared to assays without the luxOFP reference. The resulting ratiometric signal generated a clear color change from orange to teal, which can be readily captured by a smartphone (Figure 5g−i), and the mix-and-read workflow eliminated the need for multiple wash steps, facilitating rapid on-site detection.

Our biosensors effectively cover the diagnostic range of Cushing's syndrome in urine[38] and are sensitive enough to detect adrenal insufficiency after ACTH stimulation test[3] for Addison's disease diagnosis. Overall, our data demonstrate that the de novo designed cortisol luminescent biosensors, generated entirely through computational design, offer robust protein folding, high dynamic range, and sufficient sensitivity for monitoring cortisol levels relevant to individual physiology.

■ DISCUSSION

As protein design and structure prediction methods continue to evolve, all-atom models for designing and predicting complex protein−ligand interactions are becoming increasingly feasible.[39] Our analysis based on AlphaFold3 metrics revealed that it could predict ternary complex formation with higher confidence when cortisol was included, suggesting that all-atom structure prediction might potentially guide future CID development while reducing nonspecific, ligand-independent interactions. Since AlphaFold-predicted metrics correlated with the experimental target selectivity results (Figure S10c), future improvements in target selectivity may be guided by in silico design.

Traditional approaches to engineering protein biosensors often rely on empirical or semi-empirical testing of numerous variants with different linker lengths and fusion orientations.[31] By leveraging protein complex structure prediction, we can reduce the number of designs that require experimental validation from hundreds to just a few, thereby accelerating the optimization process without compromising functionality. The αLux/βit split reporter system, engineered from a de novo luciferase, has high structural predictability to allow reliable in silico modeling of biosensor architecture and ligand-induced luciferase reconstitution, leading to high-performance luminescence biosensors. In contrast, biosensors based on conven-

https://doi.org/10.1021/jacs.5c05004
J. Am. Chem. Soc. 2025, 147, 27494−27505

tional split luciferase systems often require extensive experimental fine-tuning of either swapping recognition domains, adjusting binding affinities, or optimizing domain orientations to improve the performance (Figure S11), due to limited structural predictivity.

Moving forward, our current stepwise strategy may benefit from recently developed generative models, such as RFDiffusionAA,[29,40] to enhance the design efficiency of generating heterodimer proteins that interact with user-defined ligands. Together, these advances highlight the promise of computational protein design in developing next-generation protein-based biosensors for potential diagnostics and therapeutic monitoring.

■ CONCLUSIONS

Despite the extensive development of genetically encoded protein biosensors in the past decades,[31] little is understood about the rational design of their structures and performance relationship.[41] In this study, we showcased the computational design of cortisol-responsive CID systems without relying on the re-engineering of naturally occurring proteins, resulting in the creation of de novo cortisol biosensors. By leveraging state-of-the-art protein design and structure prediction algorithms, we designed luminescent biosensors directly from the computer, which exhibited an intensiometric signal change of over 300-fold with picomolar sensitivity for cortisol detection. The intensiometric signal can be further converted into a ratiometric readout to achieve more sensitive and quantitative measurements. Furthermore, the robust luminescence produced by these biosensors is easily detectable using a standard camera, while the ratiometric color shift can be captured by smartphone imaging. This provides a user-friendly and straightforward platform for point-of-care applications, particularly given the recent progress in developing low-cost detection devices.[42,43]

■ EXPERIMENTAL METHODS

Materials and General Methods. Synthetic genes and oligonucleotides were obtained from Integrated DNA Technologies (IDT), while oligo pools were sourced from Agilent. For bacterial expression, synthetic genes were inserted into a modified Golden Gate-compatible ccdB-pET29b vector featuring a C-terminal hexahistidine tag. For yeast display, oligo pools were cloned into the pETCON plasmid. Enzymes, including restriction endonucleases, Q5 PCR polymerase, T5 exonuclease, Phusion DNA polymerase, Taq DNA ligase, and T4 ligase, were purchased from NEB. Plasmid DNA, PCR products, and digested fragments were purified by using Sydlab spin columns, and DNA sequences were verified by Azenta. The substrate, sequence information, and solvent for the αLux/βit split luciferase were acquired in the LuxSit sPro Protein:Protein Interaction System kit from Monod Bio. The substrate for LuxSit sPro was prepared as a 5 mM stock solution using the solvent provided in the kit (SP0101) and stored at −80 °C. Furimazine for the NanoBiT assay was ordered from Promega (N1110) and used at a 100× dilution. All other chemicals were purchased from Fisher Scientific, Thermo Scientific, or VWR and used as received without further purification. Size exclusion chromatography was performed using a KTA pure M system with UNICORN 7 Workstation control (GE Healthcare) coupled with a Superdex 75 Increase 10/300 GL column. DNA and protein concentrations were measured using a Take3 plate with a Biotek Synergy H1 Plate Reader. All luminescence measurements were obtained using a Biotek Synergy H1 Plate Reader with or without specified filters. Luminescence images were captured using an Amersham ImageQuant 800 and analyzed with Fiji image analysis software. No unexpected or unusually high safety hazards were encountered during the procedures.

Computational Design of Cortisol-Induced Heterodimers. Based on the site-saturation mutagenesis (SSM) map of hcy129.1, we introduced three mutations (R43I, R95Q, and Q128L) to promote hydrophobic contacts at the anticipated designable interface. Structural comparisons confirmed that these alterations preserved the original backbone and ligand-binding pocket of hcy129.1. The computational design strategy is modified from a previously described method[24] (see Figure S2). To design "lid" proteins targeting the exposed NTF2−cortisol interface, we used PatchDock to position miniprotein scaffolds in proximity to cortisol, followed by rotamer interaction field (RIF) generation for both the protein pocket and the ligand. Approximately 5 million docking configurations were evaluated using RIFdock. A preliminary step involving Rosetta ddG, ligand contact patch, and contact molecular surface predictions to reduce the designable set to 1 million docks, which were then refined via Rosetta FastDesign with cortisol explicitly included in the scoring. We retained those designs meeting these thresholds for contact molecular surface (>380), contact patch (>28), and Rosetta ddG (<−35). For the final sequence optimization, ProteinMPNN redesigned residues outside a 5 Å boundary around cortisol, preserving key ligand-contacting residues. To ensure high-confidence designs for cortisol-responsive heterodimers, the resulting sequences were then subjected to AlphaFold2 prediction under the initial guess protocol,[28] and only those with pAE < 10, pLDDT of the binder >90, contact molecular surface >440, ligand contact patch >45, and Rosetta ddG < −35 advanced to gene synthesis.

Structure Prediction and Construction of Luminescent Cortisol Biosensors. We performed structure predictions for each designed fusion sequence using a locally deployed AlphaFold3 implementation following the acquisition of AlphaFold3 model parameters upon request. The input consisted of two protein chains, with cortisol explicitly included as a defined ligand when present; otherwise, only protein chains were provided. Chain A comprised split luciferase fragment A fused via a flexible GS linker to the designed lid protein, whereas chain B consisted of split luciferase fragment B linked similarly to mhcy129 (Table S1). To ensure uniform conformational sampling, we used 8−30 model seeds for each sequence, with 5 diffusion samples per model seed. The representative structural model for subsequent analyses was determined by evaluating the average pLDDT scores computed exclusively from the nonlinker regions; specifically, the model displaying the highest mean pLDDT score within these regions was selected as the representative prediction structure. For the experimentally characterized constructs corD1-3.5GS-αLux/βitsPro-4GS-mhcy129 (±cortisol), all predicted structures from AlphaFold3 were utilized for analysis rather than solely selecting the top-ranked structure based on the pLDDT metric. A comprehensive evaluation of the distribution of these predictions was subsequently performed (Figure 5a). For detailed metric calculations, each predicted complex was partitioned into four separate fragments—split luciferase fragment A, the designed lid protein, split luciferase fragment B, and mhcy129—by removing the linker segments. The split luciferase fragment A and the designed lid protein formed a new chain A, whereas the split luciferase fragment B and mhcy129 formed a new chain B. Residue numbering of each chain started from residue 1, independently. All AlphaFold3-based analyses presented in this study were performed based on these renumbered chains A and B. The linker segments were included only for modeling purposes. Both the pLDDT and pAE metrics were extracted from the AlphaFold3 prediction outputs. Specifically, the pLDDT metric was computed at the atomic level, assigning scores to individual atoms, whereas the pAE metric was computed at the residue level, assigning scores to amino acid residues. In our complex structure, the pAE of split luciferase was computed as the mean predicted aligned error between the two fragments of the split luciferase and the CID modules' pAE as the mean predicted aligned error between the designed lid binder and mhcy129. Cα rmsd calculations were performed using a subset-based superposition method. The optimal rotation matrix was computed using the

https://doi.org/10.1021/jacs.5c05004
J. Am. Chem. Soc. 2025, 147, 27494−27505

Singular Value Decomposition of the covariance matrix. The Cα r.m.s.d. was calculated separately for different structural components: for the split luciferase modules, structure alignment was performed using split luciferase fragment A as the reference, while the displacement of split-luciferase fragment B was calculated. For the CID modules, structure alignment was performed using mhcy129 as the reference, while the displacement of the lid binder was calculated. This approach allowed for independent evaluation of structural changes in different fragments while maintaining a consistent reference frame. The final Cα rmsd values were computed as the root-mean-square of the Cartesian coordinate differences between corresponding atoms after optimal superposition. The predictions for the other hormones followed the same procedure as that for cortisol, with the only difference being the input SMILES strings for each ligand.

Yeast Display and FACS To Screen for Cortisol-Responsive Heterodimerization. A 60k yeast surface display library of the designed lid proteins was constructed according to previously reported procedures.[25] Yeast cells were induced in SGCAA medium containing 0.2% glucose, washed in PBSF, and incubated for 1 h at room temperature with 1 μM purified biotinylated mhcy129, anti-c-myc-FITC, and streptavidin-phycoerythrin (SAPE). A Sony SH800S cell sorter was used to sort five million cells based on the gating strategy shown in Figure S3b. We selected those expressed populations first for the cells without cortisol treatment and grew them for 2−3 days in C-Trp-Ura media. The cells were induced and labeled with 1 μM purified biotinylated mhcy129, anti-c-myc-FITC, streptavidin-phycoerythrin (SAPE), and 1 μM cortisol for labeling. Yeast populations with double-positive signals (anti-c-myc-FITC and SAPE) were collected and enriched for 2−3 rounds. In the final round, the collected cells were streaked on C-Trp-Ura agar plates. From these plates, 96 colonies were randomly picked, grown in C-Trp-Ura medium, and induced again in SGCAA. Each culture was then analyzed under two conditions: (1) 200 nM biotinylated mhcy129 plus anti-c-Myc-FITC and SAPE, and (2) the same plus 200 nM cortisol. Following PBSF washes, samples were analyzed on an Invitrogen Attune flow cytometer. For each clone, the cortisol-dependent change in the binding signal was measured, and clones that displayed shifts were selected. The 10 exhibiting the strongest cortisol-induced binding responses were expressed in *E. coli* for downstream characterization.

General Procedures for Protein Production and Purification. Transformed BL21 (DE3) cells carrying the gene of interest were grown at 37 °C for 18 h in LB medium supplemented with kanamycin. Cells were diluted at a 1:25 ratio in 50 mL of fresh TB medium (with kanamycin), grown at 37 °C for 3 h, and then induced by 0.5 mM IPTG for 1 h at 37 °C, followed by an additional 18 h of shaking at 25 °C. Cell pellets were collected by centrifugation at 4000*g* for 10 min and resuspended in 20 mL of lysis buffer (20 mM Tris−HCl, pH 8.0, 300 mM NaCl, 30 mM imidazole, and Pierce Protease Inhibitor Tablets). Cell resuspensions were lysed by sonication for 3 min (sonicate for 10 s and pause for 10 s per cycle; 9 cycles). Lysates were clarified by centrifugation at 15,000*g* at 12 °C for 45 min and pre-equilibrated with 600 μL of Ni-NTA nickel agarose beads at 4 °C for 30 min. The resin was washed twice with 10 mL of wash buffer (20 mM Tris−HCl pH 8.0, 300 mM NaCl, and 30 mM imidazole), followed by elution with 1.4 mL of elution buffer (20 mM Tris−HCl pH 8.0, 300 mM NaCl, and 300 mM imidazole). The eluted proteins were purified by size exclusion chromatography in 20 mM Tris−HCl, 300 mM NaCl, pH 8.0 buffer. Fractions were collected based on A280 trace, snap-frozen in liquid nitrogen, and stored at −80 °C.

Evaluation of Cortisol-Induced Dimerization by SEC. Designed lid proteins (corC6, corD11, corH12, corD2, corD7, corD1, corD10, and corC5), mhcy129, corD1-3.5GS-αLux, βitsPro-4GS-mhcy129, and mhcy129-4GS-βitsPro were expressed in *E. coli* and purified as mentioned above. Each lid protein (1 μM) was mixed with mhcy129 (1 μM) in the presence or absence of 10 μM cortisol in 1 mL of PBS, incubated at room temperature for 2 h, and loaded onto a Superdex 75 Increase 10/300 GL column pre-equilibrated with 20 mM HEPES, 50 mM NaCl (pH 7.4). corD1-3.5GS-αLux was mixed with βitsPro-4GS-mhcy129 similarly as mentioned above; instead, 20 mM Tris−HCl, 300 mM NaCl, pH 8.0 buffer was used for SEC analysis. Protein elution was monitored at 280 nm, and the resulting chromatograms were compared to detect shifts resulting from the cortisol-induced complex formation.

General In Vitro Characterization of Cortisol Biosensors. All in vitro characterizations of cortisol biosensors were carried out in white 96-well microplates (Corning 3912) in Cytiva HBS-EP+ buffer. To validate computational prediction, 10 μL of purified lid protein-αLux and mhcy129-βitsPro were prepared at 100 nM, followed by mixing with or without 10 μL of 100 μM cortisol in HBS buffer to make an 80 μL mixture. After incubating at 25 °C for 1 h for dimerization, 20 μL of 125 μM substrate from the LuxSit sPro PPI assay kit (Monod Bio, SP0101) was added, followed by measurement of luminescence signals using the Synergy H1 Plate Reader. The signal was recorded every 1 min for a total of 15 min (0.1 s integration time for every read; end point/kinetic read mode; luminescence fiber as the optic type; gain set at 120). The data from the three highest time points were used as technical triplicates. To calculate the fold of change, the average relative luminescence units (RLUs) of the technical triplicates at the final 10 μM of cortisol were divided by the RLUs signal of the no-cortisol control. To determine the dynamic range of corD1-3.5GS-αLux/βitsPro-4GS-mhcy129, corD1-3.5GS-αLux/mhcy129-4GS-βitsPro, miniH11-LgBit/mhcy129-SmBit, and corD1-LgBit/mhcy129-SmBit, a dose−response curve was carried out by mixing 10 μL of 150 nM corD1-3.5GS-αLux/βitsPro-4GS-mhcy129, corD1-3.5GS-αLux/mhcy129-4GS-βitsPro, miniH11-LgBit/mhcy129-SmBit or corD1-LgBit/mhcy129-SmBit, followed by adding 10 μL of serial diluted cortisol in 50 μL of HBS buffer. After incubating at 25 °C for 20 min, 20 μL of 125 μM substrate was added (Furimazine was used for the NanoBit system), and luminescence signals were recorded by a Plate Reader with the settings mentioned above. A dose-response curve was plotted by using the data from the three highest time points as technical triplicates. EC_{50} was calculated by fitting the curve to the dose−response-stimulation ([Agonist] vs response, variable slope) in Prism with an *R*-squared value of 0.99 for all plots. To determine the limit of detection (LOD), a reaction with the conditions mentioned above was carried out at the low end of cortisol concentrations in three different wells for triplicates. The maximum values of the triplicates were used for plotting, followed by fitting with the linear regression curve in Prism to calculate the slope. Standard error was calculated by using the STEYX equation in Excel. LOD was calculated as 3 × standard error/slope. To determine the target selectivity of corD1-3.5GS-αLux/βitsPro-4GS-mhcy129, progesterone (Thermo Fisher Scientific, AC265650050), β-estradiol (Sigma-Aldrich, E2758), and aldosterone (Sigma-Aldrich, A9477) were used to generate dose−response curves as described above.

Intensiometric and Ratiometric Cortisol Sensing in Serum and Synthetic Urine. Dose−response curves in serum and artificial urine were obtained by mixing 10 μL of 150 nM corD1-3.5GS-αLux and βitsPro-4GS-mhcy129, followed by adding 10 μL of serially diluted cortisol and 40 μL of 50% serum (Fischer Human Serum CollectTM, LOT no. 235357) or artificial urine[44] (final concentration = 20% serum or urine) in HBS buffer to make a 80 μL mixture. After incubating at 25 °C for 20 min, 20 μL of 125 μM substrate was added for luminescence signals. EC_{50}, fold of change, and LOD were calculated as mentioned above. For ratiometric cortisol sensing, reactions were carried out the same as described, except that 10 μL of 30 nM luxOFP was added as the internal reference. For signal acquisition, luminescence signals under both 508/20 and 620/40 nm channels were recorded (filter-switching per well), and the raw RLU signal under the 508 channel was divided by that under the 620 channel to obtain the 508/620 ratio for plotting and calculations of EC_{50}, fold of change, and LOD. For signal decay measurements, 15 nM corD1-3.5GS-αLux, 15 nM βitsPro-4GS-mhcy129, and 3 nM luxOFP were mixed with or without 10 μM cortisol in 20% pooled human serum. After 20 min of incubation, substrate was added and luminescence signals under both 508/20 and 620/40 nm channels were recorded for 1 h with a 30 s interval. Reactions were carried out

https://doi.org/10.1021/jacs.5c05004
J. Am. Chem. Soc. 2025, 147, 27494−27505

in three wells for technical triplicates. For plotting, the raw RLU signal under the 508 channel and the 508/620 ratio of the first time point were used for normalization.

Evaluating the Reversibility of the Designed Biosensor. The time-course luminescence kinetics was monitored in triplicate using the same instrument settings as described above. To initiate the reaction, 30 μL of a 15 nM corD1-3.5GS-αLux/βitsPro-4GS-mhcy129 mixture was combined with 30 μL of 75 μM substrate, and baseline luminescence was recorded for 5 min with a 60 s interval. To induce the dimerization of the sensor complex, 30 μL of 30 nM cortisol was added, and luminescence was monitored for an additional 10 min until the signal stabilized. To reverse dimerization, 10 μL of 2 μM purified hcy129.1 protein solution was dispensed into the reaction to compete with the sensor complex for cortisol binding, and luminescence was recorded for an additional 10 min.

Image Acquisition. Fifteen nM corD1-3.5GS-αLux, 15 nM βitsPro-4GS-mhcy129, and 4-fold serially diluted cortisol were mixed in HBS buffer, 20% synthetic urine, and 20% pooled human serum, followed by incubation at 25 °C for 20 min. Luminescence image was obtained after administration of 25 μM substrate by using ImageQuant 800 (chemiluminescence mode, binning 1 × 1, 2 s exposure). Images for ratiometric change were obtained after mixing 150 nM corD1-3.5GS-αLux, 150 nM βitsPro-4GS-mhcy129, 30 nM luxOFP, and 4-fold serially diluted cortisol. After 20 min of incubation, images were obtained using a Samsung Galaxy A33 under night mode immediately after the administration of substrate.

■ ASSOCIATED CONTENT

Supporting Information

The Supporting Information is available free of charge at https://pubs.acs.org/doi/10.1021/jacs.5c05004.

Additional sensor characterization, FACS data, AlphaFold prediction results, and sequence information (PDF)

■ AUTHOR INFORMATION

Corresponding Author

Andy Hsien-Wei Yeh − *Department of Biomolecular Engineering and Genomics Institute, University of California, Santa Cruz, California 95064, United States;* orcid.org/0000-0002-9023-776X; Email: hsyeh@ucsc.edu

Authors

Julie Yi-Hsuan Chen − *Department of Biomolecular Engineering, University of California, Santa Cruz, California 95064, United States*

Xue Peng − *Department of Biomolecular Engineering, University of California, Santa Cruz, California 95064, United States*

Chenggang Xi − *Department of Biomolecular Engineering, University of California, Santa Cruz, California 95064, United States*

Gyu Rie Lee − *Department of Biochemistry, Institute for Protein Design, and Howard Hughes Medical Institute, University of Washington, Seattle, Washington 98195, United States*

David Baker − *Department of Biochemistry, Institute for Protein Design, and Howard Hughes Medical Institute, University of Washington, Seattle, Washington 98195, United States*

Complete contact information is available at: https://pubs.acs.org/10.1021/jacs.5c05004

Author Contributions

[‖]J.Y.-H.C. and X.P. contributed equally to this work.

Funding

Research reported in this publication was supported in part by the UCSC start-up fund (C.X. and A.H.-W.Y.), NIH/NIBIB award R00EB031913 (J.Y.-H.C. and A.H.-W.Y.), Howard Hughes Medical Institute (G.R.L. and D.B.), grant 2024-337820 (J.Y.-H.C., X.P., C.X., and A.H.-W.Y.) from the Chan Zuckerberg Initiative DAF, an advised fund of Silicon Valley Community Foundation.

Notes

The authors declare the following competing financial interest(s): A.H.-W.Y., J.Y.-H.C., X.P., and D.B. are co-inventors in several provisional patent applications covering the contents described in this article. A.H.-W.Y. and D.B. are stockholders of Monod Bio.

■ ACKNOWLEDGMENTS

We thank David Baker for providing instrumental support at the Institute for Protein Design, University of Washington. Figures [1]b and S3 were partially made with BioRender.com.

■ ABBREVIATIONS

CID,chemically induced dimerization; MPNN,message passing neural network; NTF2,nuclear transport factor 2; pLDDT,predicted local distance difference test; pAE,predicted aligned error

■ REFERENCES

(1) James, K. A.; Stromin, J. I.; Steenkamp, N.; Combrinck, M. I. Understanding the Relationships between Physiological and Psychosocial Stress, Cortisol and Cognition. *Front. Endocrinol.* **2023**, *14*, No. 1085950.

(2) Nieman, L. K.; Biller, B. M. K.; Findling, J. W.; Murad, M. H.; Newell-Price, J.; Savage, M. O.; Tabarin, A. Treatment of Cushing's Syndrome: An Endocrine Society Clinical Practice Guideline. *J. Clin. Endocrinol. Metab.* **2015**, *100* (8), 2807−2831.

(3) Bornstein, S. R.; Allolio, B.; Arlt, W.; Barthel, A.; Don-Wauchope, A.; Hammer, G. D.; Husebye, E. S.; Merke, D. P.; Murad, M. H.; Stratakis, C. A.; Torpy, D. J. Diagnosis and Treatment of Primary Adrenal Insufficiency: An Endocrine Society Clinical Practice Guideline. *J. Clin. Endocrinol. Metab.* **2016**, *101* (2), 364−389.

(4) O'Byrne, N. A.; Yuen, F.; Butt, W. Z.; Liu, P. Y. Sleep and Circadian Regulation of Cortisol: A Short Review. *Curr. Opin. Endocr. Metab. Res.* **2021**, *18*, 178−186.

(5) Iqbal, T.; Elahi, A.; Wijns, W.; Shahzad, A. Cortisol Detection Methods for Stress Monitoring in Connected Health. *Health Sci. Rev.* **2023**, *6*, No. 100079.

(6) Vignesh, V.; Castro-Dominguez, B.; James, T. D.; Gamble-Turner, J. M.; Lightman, S.; Reis, N. M. Advancements in Cortisol Detection: From Conventional Methods to next-Generation Technologies for Enhanced Hormone Monitoring. *ACS Sens.* **2024**, *9* (4), 1666−1681.

(7) Ni, Y.; Rosier, B. J. H. M.; van Aalen, E. A.; Hanckmann, E. T. L.; Biewenga, L.; Pistikou, A.-M. M.; Timmermans, B.; Vu, C.; Roos, S.; Arts, R.; Li, W.; de Greef, T. F. A.; van Borren, M. M. G. J.; van Kuppeveld, F. J. M.; Bosch, B.-J.; Merkx, M. A Plug-and-Play Platform of Ratiometric Bioluminescent Sensors for Homogeneous Immunoassays. *Nat. Commun.* **2021**, *12* (1), 4586.

(8) Quijano-Rubio, A.; Yeh, H. W.; Park, J.; Lee, H.; Langan, R. A.; Boyken, S. E.; Lajoie, M. J.; Cao, L. X.; Chow, C. M.; Miranda, M. C.; Wi, J.; Hong, H. J.; Stewart, L.; Oh, B. H.; Baker, D. De Novo Design of Modular and Tunable Protein Biosensors. *Nature* **2021**, *591* (7850), 482−487.

(9) Zhang, J. Z.; Yeh, H.-W.; Walls, A. C.; Wicky, B. I. M.; Sprouse, K. R.; VanBlargan, L. A.; Treger, R.; Quijano-Rubio, A.; Pham, M. N.; Kraft, J. C.; Haydon, I. C.; Yang, W.; DeWitt, M.; Bowen, J. E.; Chow, C. M.; Carter, L.; Ravichandran, R.; Wener, M. H.; Stewart, L.;

Veesler, D.; Diamond, M. S.; Greninger, A. L.; Koelle, D. M.; Baker, D. Thermodynamically Coupled Biosensors for Detecting Neutralizing Antibodies against SARS-CoV-2 Variants. *Nat. Biotechnol.* **2022**, *40* (9), 1336−1340.

(10) Yeh, H.-W.; Ai, H.-W. Development and Applications of Bioluminescent and Chemiluminescent Reporters and Biosensors. *Annu. Rev. Anal. Chem.* **2019**, *12* (1), 129−150.

(11) Arts, R.; den Hartog, I.; Zijlema, S. E.; Thijssen, V.; van der Beelen, S. H. E.; Merkx, M. Detection of Antibodies in Blood Plasma Using Bioluminescent Sensor Proteins and a Smartphone. *Anal. Chem.* **2016**, *88* (8), 4525−4532.

(12) Tenda, K.; van Gerven, B.; Arts, R.; Hiruta, Y.; Merkx, M.; Citterio, D. Paper-based Antibody Detection Devices Using Bioluminescent BRET-switching Sensor Proteins. *Angew. Chem. Weinheim Bergstr. Ger.* **2018**, *130* (47), 15595−15599.

(13) Gardill, B. R.; Vogl, M. R.; Lin, H.-Y.; Hammond, G. L.; Muller, Y. A. Corticosteroid-Binding Globulin: Structure-Function Implications from Species Differences. *PLoS One* **2012**, *7* (12), No. e52759.

(14) Lockett, J.; Inder, W. J.; Clifton, V. L. The Glucocorticoid Receptor: Isoforms, Functions, and Contribution to Glucocorticoid Sensitivity. *Endocr. Rev.* **2024**, *45* (4), 593−624.

(15) Stanton, B. Z.; Chory, E. J.; Crabtree, G. R. Chemically induced proximity in biology and medicine. *Science* **2018**, *359* (6380), No. eaao5902.

(16) Banaszynski, L. A.; Liu, C. W.; Wandless, T. J. Characterization of the FKBP·rapamycin·FRB Ternary Complex [J. Am. Chem. Soc. 2005, 127, 4715−4721]. *J. Am. Chem. Soc.* **2006**, *128* (49), 15928−15928.

(17) Liang, F.-S.; Ho, W. Q.; Crabtree, G. R. Engineering the ABA Plant Stress Pathway for Regulation of Induced Proximity. *Sci. Signal.* **2011**, *4* (164), rs2.

(18) Miyamoto, T.; DeRose, R.; Suarez, A.; Ueno, T.; Chen, M.; Sun, T.-P.; Wolfgang, M. J.; Mukherjee, C.; Meyers, D. J.; Inoue, T. Rapid and Orthogonal Logic Gating with a Gibberellin-Induced Dimerization System. *Nat. Chem. Biol.* **2012**, *8* (5), 465−470.

(19) Glasgow, A. A.; Huang, Y.-M.; Mandell, D. J.; Thompson, M.; Ritterson, R.; Loshbaugh, A. L.; Pellegrino, J.; Krivacic, C.; Pache, R. A.; Barlow, K. A.; Ollikainen, N.; Jeon, D.; Kelly, M. J. S.; Fraser, J. S.; Kortemme, T. Computational Design of a Modular Protein Sense-Response System. *Science* **2019**, *366* (6468), 1024−1028.

(20) Zajc, C. U.; Dobersberger, M.; Schaffner, I.; Mlynek, G.; Pühringer, D.; Salzer, B.; Djinović-Carugo, K.; Steinberger, P.; De Sousa Linhares, A.; Yang, N. J.; Obinger, C.; Holter, W.; Traxlmayr, M. W.; Lehner, M. A Conformation-Specific ON-Switch for Controlling CAR T Cells with an Orally Available Drug. *Proc. Natl. Acad. Sci. U. S. A.* **2020**, *117* (26), 14926−14935.

(21) Foight, G. W.; Wang, Z.; Wei, C. T.; Greisen, P., Jr; Warner, K. M.; Cunningham-Bryant, D.; Park, K.; Brunette, T. J.; Sheffler, W.; Baker, D.; Maly, D. J. Multi-Input Chemical Control of Protein Dimerization for Programming Graded Cellular Responses. *Nat. Biotechnol.* **2019**, *37* (10), 1209−1216.

(22) Marchand, A.; Buckley, S.; Schneuing, A.; Pacesa, M.; Elia, M.; Gainza, P.; Elizarova, E.; Neeser, R. M.; Lee, P.-W.; Reymond, L.; Miao, Y.; Scheller, L.; Georgeon, S.; Schmidt, J.; Schwaller, P.; Maerkl, S. J.; Bronstein, M.; Correia, B. E. Targeting Protein−Ligand Neosurfaces with a Generalizable Deep Learning Tool. *Nature* **2025**, *639*, 522.

(23) An, L.; Said, M.; Tran, L.; Majumder, S.; Goreshnik, I.; Lee, G. R.; Juergens, D.; Dauparas, J.; Anishchenko, I.; Coventry, B.; Bera, A. K.; Kang, A.; Levine, P. M.; Alvarez, V.; Pillai, A.; Norn, C.; Feldman, D.; Zorine, D.; Hicks, D. R.; Li, X.; Sanchez, M. G.; Vafeados, D. K.; Salveson, P. J.; Vorobieva, A. A.; Baker, D. Binding and Sensing Diverse Small Molecules Using Shape-Complementary Pseudocycles. *Science* **2024**, *385* (6706), 276−282.

(24) Lee, G. R.; Pellock, S. J.; Norn, C.; Tischer, D.; Dauparas, J.; Anischenko, I.; Mercer, J. A. M.; Kang, A.; Bera, A.; Nguyen, H.; Goreshnik, I.; Vafeados, D.; Roullier, N.; Han, H. L.; Coventry, B.; Haddox, H. K.; Liu, D. R.; Yeh, A. H.-W.; Baker, D. Small-Molecule Binding and Sensing with a Designed Protein Family. *bioRxiv*, **2023**.

(25) Cao, L.; Coventry, B.; Goreshnik, I.; Huang, B.; Sheffler, W.; Park, J. S.; Jude, K. M.; Marković, I.; Kadam, R. U.; Verschueren, K. H. G.; Verstraete, K.; Walsh, S. T. R.; Bennett, N.; Phal, A.; Yang, A.; Kozodoy, L.; DeWitt, M.; Picton, L.; Miller, L.; Strauch, E.-M.; DeBouver, N. D.; Pires, A.; Bera, A. K.; Halabiya, S.; Hammerson, B.; Yang, W.; Bernard, S.; Stewart, L.; Wilson, I. A.; Ruohola-Baker, H.; Schlessinger, J.; Lee, S.; Savvides, S. N.; Garcia, K. C.; Baker, D. Design of Protein-Binding Proteins from the Target Structure Alone. *Nature* **2022**, *605* (7910), 551−560.

(26) Dauparas, J.; Anishchenko, I.; Bennett, N.; Bai, H.; Ragotte, R. J.; Milles, L. F.; Wicky, B. I. M.; Courbet, A.; de Haas, R. J.; Bethel, N.; Leung, P. J. Y.; Huddy, T. F.; Pellock, S.; Tischer, D.; Chan, F.; Koepnick, B.; Nguyen, H.; Kang, A.; Sankaran, B.; Bera, A. K.; King, N. P.; Baker, D. Robust Deep Learning-Based Protein Sequence Design Using ProteinMPNN. *Science* **2022**, *378* (6615), 49−56.

(27) Jumper, J.; Evans, R.; Pritzel, A.; Green, T.; Figurnov, M.; Ronneberger, O.; Tunyasuvunakool, K.; Bates, R.; Zidek, A.; Potapenko, A.; Bridgland, A.; Meyer, C.; Kohl, S. A. A.; Ballard, A. J.; Cowie, A.; Romera-Paredes, B.; Nikolov, S.; Jain, R.; Adler, J.; Back, T.; Petersen, S.; Reiman, D.; Clancy, E.; Zielinski, M.; Steinegger, M.; Pacholska, M.; Berghammer, T.; Bodenstein, S.; Silver, D.; Vinyals, O.; Senior, A. W.; Kavukcuoglu, K.; Kohli, P.; Hassabis, D. Highly Accurate Protein Structure Prediction with AlphaFold. *Nature* **2021**, *596* (7873), 583−589.

(28) Bennett, N. R.; Coventry, B.; Goreshnik, I.; Huang, B.; Allen, A.; Vafeados, D.; Peng, Y. P.; Dauparas, J.; Baek, M.; Stewart, L.; DiMaio, F.; De Munck, S.; Savvides, S. N.; Baker, D. Improving de Novo Protein Binder Design with Deep Learning. *Nat. Commun.* **2023**, *14* (1), 2625.

(29) Krishna, R.; Wang, J.; Ahern, W.; Sturmfels, P.; Venkatesh, P.; Kalvet, I.; Lee, G. R.; Morey-Burrows, F. S.; Anishchenko, I.; Humphreys, I. R.; McHugh, R.; Vafeados, D.; Li, X.; Sutherland, G. A.; Hitchcock, A.; Hunter, C. N.; Kang, A.; Brackenbrough, E.; Bera, A. K.; Baek, M.; DiMaio, F.; Baker, D. Generalized Biomolecular Modeling and Design with RoseTTAFold All-Atom. *Science* **2024**, *384* (6693), No. eadl2528.

(30) Abramson, J.; Adler, J.; Dunger, J.; Evans, R.; Green, T.; Pritzel, A.; Ronneberger, O.; Willmore, L.; Ballard, A. J.; Bambrick, J.; Bodenstein, S. W.; Evans, D. A.; Hung, C.-C.; O'Neill, M.; Reiman, D.; Tunyasuvunakool, K.; Wu, Z.; Žemgulytė, A.; Arvaniti, E.; Beattie, C.; Bertolli, O.; Bridgland, A.; Cherepanov, A.; Congreve, M.; Cowen-Rivers, A. I.; Cowie, A.; Figurnov, M.; Fuchs, F. B.; Gladman, H.; Jain, R.; Khan, Y. A.; Low, C. M. R.; Perlin, K.; Potapenko, A.; Savy, P.; Singh, S.; Stecula, A.; Thillaisundaram, A.; Tong, C.; Yakneen, S.; Zhong, E. D.; Zielinski, M.; Žídek, A.; Bapst, V.; Kohli, P.; Jaderberg, M.; Hassabis, D.; Jumper, J. M. Accurate Structure Prediction of Biomolecular Interactions with AlphaFold 3. *Nature* **2024**, *630*, 493.

(31) Gest, A. M. M.; Sahan, A. Z.; Zhong, Y.; Lin, W.; Mehta, S.; Zhang, J. Molecular Spies in Action: Genetically Encoded Fluorescent Biosensors Light up Cellular Signals. *Chem. Rev.* **2024**, *124* (22), 12573−12660.

(32) Das, D.; Ainavarapu, S. R. K. Protein Engineering Using Circular Permutation - Structure, Function, Stability, and Applications. *FEBS J.* **2024**, *291* (16), 3581−3596.

(33) Dixon, A. S.; Schwinn, M. K.; Hall, M. P.; Zimmerman, K.; Otto, P.; Lubben, T. H.; Butler, B. L.; Binkowski, B. F.; Machleidt, T.; Kirkland, T. A.; Wood, M. G.; Eggers, C. T.; Encell, L. P.; Wood, K. V. NanoLuc Complementation Reporter Optimized for Accurate Measurement of Protein Interactions in Cells. *ACS Chem. Biol.* **2016**, *11* (2), 400−408.

(34) Yeh, A. H.-W.; Norn, C.; Kipnis, Y.; Tischer, D.; Pellock, S. J.; Evans, D.; Ma, P.; Lee, G. R.; Zhang, J. Z.; Anishchenko, I.; Coventry, B.; Cao, L.; Dauparas, J.; Halabiya, S.; DeWitt, M.; Carter, L.; Houk, K. N.; Baker, D. De Novo Design of Luciferases Using Deep Learning. *Nature* **2023**, *614* (7949), 774−780.

(35) Vergara, R.; Wagner, J.; Kamalian, P.; Harman, J. L.; Lara, N.; Fischer, E. S.; Bernardes, G. J. L.; Quijano-Rubio, A.; Silva, D. A. LuxSit Pro and sPro: Next-Generation Designed Luciferases for

Bioluminescent Reporting and Complementation-Based Detection. *bioRxiv* **2025**, DOI: 10.1101/2025.07.21.665742.
(36) Halbers, L. P.; Cole, K. H.; Ng, K. K.; Fuller, E. B.; Chan, C. E. T.; Callicoatte, C.; Metcalfe, M.; Chen, C. C.; Barhoosh, A. A.; Reid-McLaughlin, E.; Kent, A. D.; Torrey, Z. R.; Steward, O.; Lupták, A.; Prescher, J. A. A Modular Platform for Bioluminescent RNA Tracking. *Nat. Commun.* **2024**, *15* (1), 9992.
(37) Chen, J. Y.-H.; Shi, Q.; Peng, X.; Habimana, J. de D.; Wang, J.; Sobolewski, W.; Yeh, A. H.-W. De Novo Luciferases Enable Multiplexed Bioluminescence Imaging. *Chem.* **2025**, *11*, 102346.
(38) Fleseriu, M.; Auchus, R.; Bancos, I.; Ben-Shlomo, A.; Bertherat, J.; Biermasz, N. R.; Boguszewski, C. L.; Bronstein, M. D.; Buchfelder, M.; Carmichael, J. D.; Casanueva, F. F.; Castinetti, F.; Chanson, P.; Findling, J.; Gadelha, M.; Geer, E. B.; Giustina, A.; Grossman, A.; Gurnell, M.; Ho, K.; Ioachimescu, A. G.; Kaiser, U. B.; Karavitaki, N.; Katznelson, L.; Kelly, D. F.; Lacroix, A.; McCormack, A.; Melmed, S.; Molitch, M.; Mortini, P.; Newell-Price, J.; Nieman, L.; Pereira, A. M.; Petersenn, S.; Pivonello, R.; Raff, H.; Reincke, M.; Salvatori, R.; Scaroni, C.; Shimon, I.; Stratakis, C. A.; Swearingen, B.; Tabarin, A.; Takahashi, Y.; Theodoropoulou, M.; Tsagarakis, S.; Valassi, E.; Varlamov, E. V.; Vila, G.; Wass, J.; Webb, S. M.; Zatelli, M. C.; Biller, B. M. K. Consensus on Diagnosis and Management of Cushing's Disease: A Guideline Update. *Lancet Diabetes Endocrinol.* **2021**, *9* (12), 847−875.
(39) Albanese, K. I.; Barbe, S.; Tagami, S.; Woolfson, D. N.; Schiex, T. Computational Protein Design. *Nat. Rev. Methods Primers* **2025**, *5* (1), 13.
(40) Kim, D.; Woodbury, S. M.; Ahern, W.; Kalvet, I.; Hanikel, N.; Salike, S.; Pellock, S. J.; Lauko, A.; Hilvert, D.; Baker, D. Computational Design of Metallohydrolases. *bioRxiv*, **2024**.
(41) Rosen, P. C.; Horwitz, S. M.; Brooks, D. J.; Kim, E.; Ambarian, J. A.; Waidmann, L.; Davis, K. M.; Yellen, G. State-Dependent Motion of a Genetically Encoded Fluorescent Biosensor. *Proc. Natl. Acad. Sci. U. S. A.* **2025**, *122* (10), No. e2426324122.
(42) Tomimuro, K.; Tenda, K.; Ni, Y.; Hiruta, Y.; Merkx, M.; Citterio, D. Thread-Based Bioluminescent Sensor for Detecting Multiple Antibodies in a Single Drop of Whole Blood. *ACS Sens.* **2020**, *5* (6), 1786−1794.
(43) Boitet, M.; Eun, H.; Achek, A.; Carla de Almeida Falcão, V.; Delorme, V.; Grailhe, R. Biolum' RGB: A Low-Cost, Versatile, and Sensitive Bioluminescence Imaging Instrument for a Broad Range of Users. *ACS Sens.* **2022**, *7* (9), 2556−2566.
(44) Chutipongtanate, S.; Thongboonkerd, V. Systematic Comparisons of Artificial Urine Formulas for in Vitro Cellular Study. *Anal. Biochem.* **2010**, *402* (1), 110−112.